Development 138, 1131-1142 (2011) doi:10.1242/dev.058149

Pkd1l1 establishes left-right asymmetry and physically interacts with Pkd2

Sarah Field*, Kerry-Lyn Riley*, Daniel T. Grimes*, Helen Hilton, Michelle Simon, Nicola Powles-Glover, Pam Siggers, Debora Bogani, Andy Greenfield and Dominic P. Norris†

SUMMARY

In mammals, left-right (L-R) asymmetry is established by posteriorly oriented cilia driving a leftwards laminar flow in the embryonic node, thereby activating asymmetric gene expression. The two-cilia hypothesis argues that immotile cilia detect and respond to this flow through a Pkd2-mediated mechanism; a putative sensory partner protein has, however, remained unidentified. We have identified the *Pkd1*-related locus *Pkd1l1* as a crucial component of L-R patterning in mouse. Systematic comparison of *Pkd1l1* and *Pkd2* point mutants reveals strong phenocopying, evidenced by both morphological and molecular markers of sidedness; both mutants fail to activate asymmetric gene expression at the node or in the lateral plate and exhibit right isomerism of the lungs. Node and cilia morphology were normal in mutants and cilia demonstrated typical motility, consistent with Pkd1l1 and Pkd2 activity downstream of nodal flow. Cell biological analysis reveals that Pkd1l1 and Pkd2 localise to the cilium and biochemical experiments demonstrate that they can physically interact. Together with co-expression in the node, these data argue that Pkd1l1 is the elusive Pkd2 binding partner required for L-R patterning and support the two-cilia hypothesis.

KEY WORDS: Left-right asymmetry, Polycystin, Cilia, Mouse

INTRODUCTION

The internal organs and vasculature of all vertebrates are left-right (L-R) asymmetrical in their position and patterning; this asymmetry is conserved, revealing a clearly ancient origin. Morphological asymmetry of the initially symmetrical embryo is first evident during somitogenesis, when the heart tube kinks asymmetrically to the right. During subsequent development of the embryo, the heart, lungs, gut and associated vasculature all become asymmetrically positioned and patterned. Defects in this process are associated with congenital human disorders, most significantly heart disease (Ramsdell, 2005).

The earliest known event in establishing mammalian L-R asymmetry is a leftwards flow of liquid in the embryonic node, at ~8.0 days post-coitum (dpc) in mouse, resulting from the clockwise rotation of polarised, posteriorly tilted nodal cilia (Hirokawa et al., 2006; Shiratori and Hamada, 2006). This 'nodal flow' in turn results in activation of the left-sided Nodal signalling cascade. The TGFβ family member *Nodal* is expressed in the left, but not right, lateral plate mesoderm (LPM) (Collignon et al., 1996; Lowe et al., 1996), where it induces its own expression, as well as that of its antagonist *Lefty2* and the downstream transcription factor *Pitx2* (Shiratori and Hamada, 2006). Whereas *Nodal* and *Lefty2* are expressed for only a few hours (between 3 and 6 somites), specifically left-sided *Pitx2* expression is maintained into organogenesis and is argued to be the ultimate specifier of leftness (Logan et al., 1998; Ryan et al., 1998).

Mammalian Genetics Unit, MRC Harwell, Harwell Science and Innovation Campus, Oxfordshire OX11 0RD, UK.

*These authors contributed equally to this work
†Author for correspondence (d.norris@har.mrc.ac.uk)

Accepted 10 January 2011

Although it is broadly accepted that nodal flow drives asymmetric gene expression in the mouse (Hirokawa et al., 2006; Nonaka et al., 2002; Shiratori and Hamada, 2006), the mechanism by which flow is detected, and the nature of the response at the tissue and cellular level, remain unclear. An initial hypothesis argued that a morphogen becomes concentrated on the left side of the node in response to flow (Nonaka et al., 2002; Okada et al., 1999; Okada et al., 2005). Others suggested that Nodal itself is asymmetrically transported towards the left lateral plate in response to flow (Brennan et al., 2002; Oki et al., 2007; Saijoh et al., 2003). In a development of these theories, Tanaka and colleagues argued that lipid-bound vesicles containing morphogens are carried leftwards, breaking on the left side of the node and thereby releasing their cargoes asymmetrically (Tanaka et al., 2005). By contrast, the two-cilia hypothesis (McGrath et al., 2003; Tabin and Vogan, 2003) proposed that, in addition to motile cilia creating flow, immotile mechanosensory cilia within the node are displaced and respond to flow on the left, but not right, side of the node. It has been proposed that this results in a left-sided Ca^{2+} signal through the action of Pkd2 (McGrath et al., 2003).

The *PKD1* and *PKD2* genes were identified as being mutated in human autosomal dominant polycystic kidney disease (OMIM: 173900) (Harris and Torres, 2009). Work from various groups has led to the understanding that these two proteins act together, forming a flow-sensitive Ca^{2+} channel in kidney tubules (Hanaoka et al., 2000; Nauli et al., 2003). PKD1, which contains a large and structurally robust extracellular domain, is believed to act as a flow sensor, whereas PKD2 forms the channel (Gonzalez-Perrett et al., 2001; Koulen et al., 2002). Loss-of-function mouse mutants of *Pkd1* and *Pkd2* are homozygous lethal, resulting in embryonic death associated with cardiac failure, polycystic kidneys and gross oedema (Boulter et al., 2001; Lu et al., 2001; Muto et al., 2002; Pennekamp et al., 2002; Wu et al., 2000). Heterozygous mutants of both *Pkd1* and *Pkd2* survive to adulthood, but show adult-onset

polycystic kidney disease, a phenotype that develops earlier in double than single heterozygotes (Wu et al., 2002). Homozygous *Pkd2* mutants also show distinct L-R patterning defects, failing to activate detectable levels of *Nodal* expression in the lateral plate (Pennekamp et al., 2002); these data underpin the two-cilia hypothesis that nodal flow activates Pkd2 signalling specifically on the left side of the node (McGrath et al., 2003). Surprisingly, no overt L-R patterning defects are evident in the mouse *Pkd1* mutant, and Pkd1 protein was not detected in the rabbit node (Karcher et al., 2005), suggesting that *Pkd2* acts in L-R determination in the absence of Pkd1 protein; there are, however, conflicting data concerning the presence of Pkd1 in the mouse node (Karcher et al., 2005; Nakaya et al., 2005). Although it is formally possible that Pkd2 acts alone in L-R determination, other binding partners, such as inversin, have been suggested (Karcher et al., 2005).

Here, we report the identification of a point mutation in the mouse *Pkd1l1* locus named *rks* that results in right pulmonary isomerism, cardiac outflow defects, overt oedema and lethality by 15.5 dpc. The normally left-sided genes *Nodal*, *Lefty2* and *Pitx2* are not expressed in *Pkd1l1*^{rks} mutants, indicating a failure to activate the Nodal signalling cascade. Node morphology, cilia morphology and cilia motility are all unaffected in *Pkd1l1*^{rks} mutants. Systematic analysis of a *Pkd2* mutant on an identical genetic background shows that *Pkd1l1* and *Pkd2* mutants phenocopy, suggesting that Pkd1l1 is the elusive Pkd2 binding partner in L-R determination. We demonstrate that Pkd1l1 can directly interact with Pkd2 and that, when co-expressed, both proteins localise to the cilium. We propose that direct interaction between Pkd1l1 and Pkd2 is required for L-R determination, thereby supporting the two-cilia hypothesis.

MATERIALS AND METHODS

Mice

Pkd1l1^{rks} was derived from an ENU-driven genetic screen; mutagenised C57Bl6/J mice were outcrossed to C3H/HeH. The line was maintained by backcrossing to C3H/HeH. *Pkd2*^{lrm4} is an E442G point mutation, previously incorrectly described as being E452G (Ermakov et al., 2009), and was maintained by backcrossing to C3H/HeH. Genotyping of mutant single-nucleotide polymorphisms (SNPs) was performed by pyrosequencing.

DNA constructs

Full-length *Pkd1l1* cDNA was synthesised according to NCBI ref. seq. XM_126005.7. The Pkd1l1_CC fragment comprised bases 7320-7821 (amino acids 2440-2607). The whole-mount in situ hybridisation probe comprised bases 5245-6073. Both full-length *Pkd1l1* cDNA and Pkd1l1_CC were C-terminally tagged with GFP by cloning into pEGFP-N1 (Clontech). Pkd1l1_CC^{L2554D}-GFP was produced using the QuikChange mutagenesis kit (Stratagene). The Myc-PKD2 vector was as previously described (Hanaoka et al., 2000).

Whole-mount in situ hybridisation (WISH)

WISH was performed using standard protocols. Digoxygenin-labelled riboprobes for *Pkd1l1*, *Pkd2* (Pennekamp et al., 2002), *Nodal* (Collignon et al., 1996), *Lefty1/2* (Meno et al., 1997), *Pitx2* (Ryan et al., 1998), *Twist* (*Twist1*) (Fuchtbauer, 1995), *Cerl2* (Marques et al., 2004) and *Shh* (Echelard et al., 1993) were transcribed. Alkaline phosphatase-coupled anti-digoxygenin antibody (Roche) was used to localise hybridised probes and NBT/BCIP (Roche) was the chromogenic substrate, producing blue precipitates for visualisation.

Analysis of embryonic nodes

For morphological analysis, embryos were fixed in 2% glutaraldehyde, dehydrated through an acetone series, critical-point dried (EMITECH 850), mounted, sputter coated with gold (8 nm) and viewed in a Hitachi S-530 or JEOL 6500F scanning electron microscope. For cilia beat analysis, embryos dissected in ice-cold 199 medium (GIBCO) were flat-mounted on a microscope slide under a coverslip. High-speed video capture (100 frames per second) was performed under differential interference contrast optics (Leica 2500 microscope) using a 63× NA 0.9 objective. At least four wild-type and mutant embryos were analysed frame-by-frame; six different cilia per node were counted for five rotations to calculate rotation frequency. Yolk sacs were collected for genotyping.

Cell culture, transfection and immunofluorescence

HEK 293T cells were maintained in DMEM (Invitrogen) and IMCD3 cells in DMEM/F12 (Invitrogen) media, both supplemented with 10% foetal bovine serum (Invitrogen), pen-strep (Invitrogen) and L-glutamine (Invitrogen). Constructs were transfected using JetPei (Polypus Transfection) according to the manufacturer's instructions. For immunofluorescence, GFP and Myc protein tags were detected using rabbit anti-GFP (1:1000; Invitrogen, A-21311) and mouse anti-Myc (1:200; Hybridoma Bank, 9E10) antibodies, respectively. Alexa Fluor 488 nm, 594 nm and 647 nm secondary antibodies (Invitrogen, A11032, A21206 and A21463) were used for visualisation. Slides were imaged using a TCS SP5 confocal microscope (Leica). Cilia were visualised using an antibody against acetylated tubulin (1:1000; Sigma, T7451).

Protein preparation, Western blotting and immunoprecipitation

Cells were lysed in RIPA buffer supplemented with Protease Inhibitor Cocktail (Roche). Total protein concentration was determined using Bradford Reagent (Sigma). Immunoprecipitations (IPs) were performed with 0.4 mg pre-cleared protein lysate per IP, using anti-Myc (Sigma, C 3956) and anti-GFP (Roche, 11 814 460 001) antibodies bound to Protein G Sepharose beads (Sigma, P3296). IPs were performed for 1 hour at 4°C with rotation. Precipitates were resolved on 4-12% Bis-Tris gels (Invitrogen), transferred onto nitrocellulose membranes (iBLOT; Invitrogen), then blocked in 5% milk in PBT (0.1% Tween 20 in PBS). Membranes were probed with anti-GFP (1:4000; Roche, 11 814 460 001) or anti-Myc (1:5000; Hybridoma Bank, 9E10) antibodies.

Sequence alignment and molecular modelling

Multiple sequence alignment was performed with ClustalW and visualised with JalView. Molecular modelling was performed using nFOLD3 (Jones et al., 2005). Structures were rendered using PyMol (http://www.pymol.org/).

RESULTS

rks: a novel *Pkd1l1* allele in mouse

During an ongoing ENU-driven forward genetic screen for developmental defects in mouse (Bogani et al., 2009; Patterson et al., 2009; Yates et al., 2009), a recessive mutant demonstrating consistent situs abnormalities was identified. Right pulmonary isomerism and gross oedema were evident in all phenotypic individuals from the initial screen, together with apparently randomised situs of other organ systems (data not shown). We named this mutant rikishi (*rks*) owing to the similarity in shape of the initial mutants to a Sumo wrestler. A genome-wide analysis of 11 such phenotypic G3 embryos demonstrated linkage of *rks* to proximal chromosome 11 (data not shown). Successive backcrossing to C3H/HeH mice was accompanied by intercrosses to produce further phenotypic embryos for mapping. Subsequent haplotypic analyses defined a ~200 kb minimal region between 8.69 and 8.89 Mb as containing the mutation; multiple recombination events at both flanking markers were recorded (Fig. 1A).

The *rks* minimal region contains only the *Pkd1l1* locus and two non-coding pseudogenes (Fig. 1A). As *Pkd1l1* is the only functional gene in the region, and because the gross phenotype of *rks* appeared strikingly similar to that of the well-characterised *Pkd2* null (Pennekamp et al., 2002), we hypothesised that Pkd1l1 might be the elusive Pkd2 binding partner. We therefore sequenced

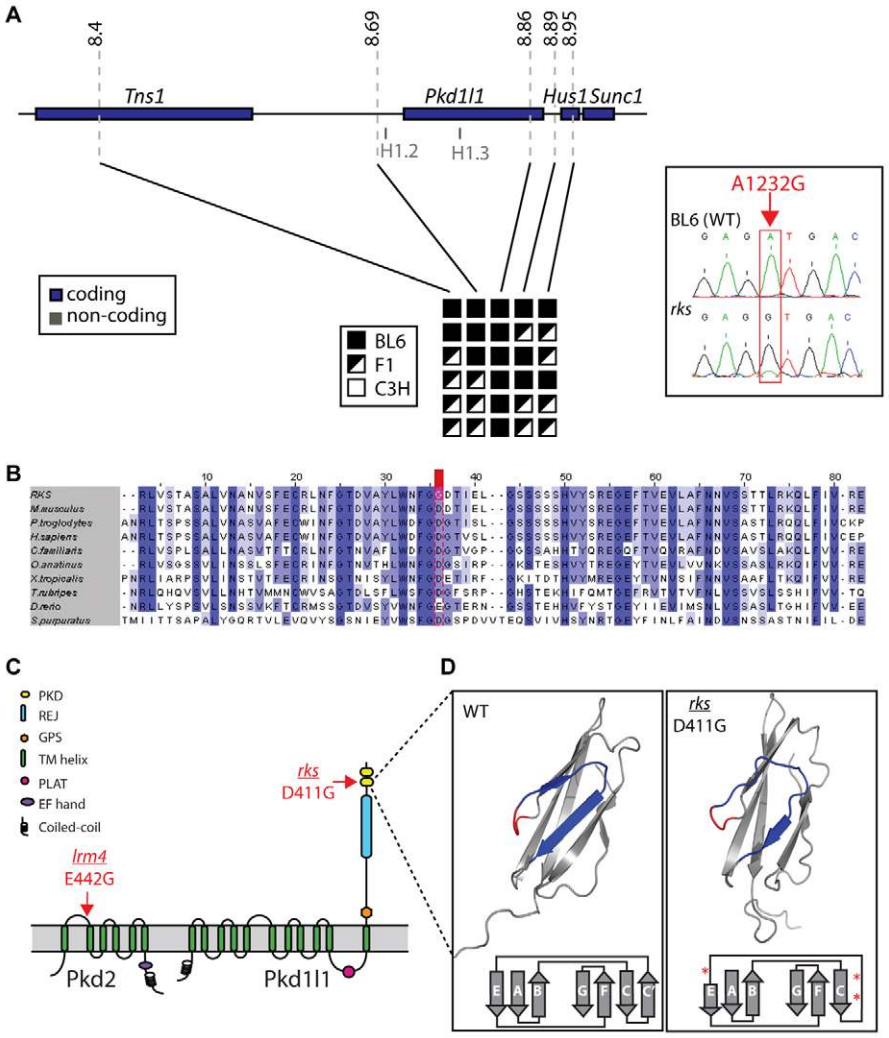

Fig. 1. *rks* disrupts a PKD domain of Pkd1l1. (**A**) The *rks* mutation maps to a ~200 kb region on mouse chromosome 11 containing the *Pkd1l1* locus and two non-coding pseudogenes. Recombination events at flanking markers were recorded. Sequencing of the critical region revealed an A-to-G transition at nucleotide 1232 in exon 8 of *Pkd1l1* (box). (**B**) Multiple sequence alignment of orthologous PKD domains with the *Pkd1l1*^{rks} point mutation in the conserved WDFDGDS motif highlighted (red). (**C**) Domain structure and membrane topology of mouse Pkd2 and Pkd1l1 with the *Pkd2*^{lrm4} and *Pkd1l1*^{rks} amino acid substitutions indicated (red arrows). (**D**) Wild-type (WT) and *Pkd1l1*^{rks} mutant PKD domains modelled using nFOLD3. A schematic of the domains is given beneath. In the mutant, the C′ and much of the E β-sheets are destabilised (asterisks).

all the exons of *Pkd1l1*, the associated splice donor and acceptor sites and the non-coding pseudogenes. A single sequence change from the reference was detected in exon 8 of *Pkd1l1*, at nucleotide 1232 (Fig. 1A). This A-to-G transition results in a negatively charged aspartic acid at position 411 being replaced by an uncharged non-polar glycine residue; the changes in charge and size are both non-conservative in nature.

The Pkd1l1 protein comprises 11 transmembrane domains, a C-terminal intracellular coiled coil (see Fig. S1 in the supplementary material) and an N-terminal extracellular region encompassing a REJ domain and two PKD domains (Fig. 1C) (Yuasa et al., 2002); the *Pkd1l1*^{rks} mutation lies in the second PKD domain. Multi-species amino acid alignment revealed a high level of conservation within the domain, with absolute conservation of the mutated residue seen in species as distantly related as the sea urchin (*S. pupuratus*); a conservative change to the negatively charged glutamic acid is present in zebrafish (Fig. 1B). Previous analysis of equivalent domains in Pkd1 identified the WDFGDGS motif, within which the *Pkd1l1*^{rks} mutation (underlined) lies, as the most highly conserved region of the domain (Fig. 1B) (Bycroft et al., 1999). Both NMR-derived and X-ray crystallography-derived structures of PKD domains comprise β-sandwiches of seven β-sheets (Bycroft et al., 1999; Jing et al., 2002); the WDFGDGS motif forms a linker connecting β-sheets C and C′ (Fig. 1D). Based on these structures, we modelled the likely effects of the *Pkd1l1*^{rks} mutation using homology-based molecular modelling with nFOLD3 (Jones et al., 2005). This yielded an in silico prediction of destabilisation of the C′ β-sheet and a reduction of the length of the E β-sheet (Fig. 1D), implying that the *Pkd1l1*^{rks} phenotype results from structural disruption of the second PKD domain of Pkd1l1.

Pkd1l1^{rks} mutants exhibit gross left-right abnormalities that phenocopy *Pkd2*^{lrm4} mutants

Although initial analysis during screening gave an indication of the *Pkd1l1*^{rks} phenotype, these embryos were of mixed genetic background and were likely to carry additional, unknown ENU-derived mutations. Moreover, non-phenotypic embryos were not genotyped for the *Pkd1l1*^{rks} mutation, hence genetic penetrance was undetermined. The previously reported *Pkd2*^{lrm4} point mutant, a predicted null allele, was also originally analysed on a mixed genetic background (Ermakov et al., 2009). Therefore, both the *Pkd1l1*^{rks} and *Pkd2*^{lrm4} mutations were backcrossed to C3H for over ten generations, segregating away other ENU-derived mutations and providing a single, defined genetic background. The resulting congenic stocks were analysed in this study. Initially, we assessed age of death for *Pkd1l1*^{rks}, collecting and genotyping cohorts of embryos at 13.5, 14.5 and 15.5 dpc (Fig. 2J). At both

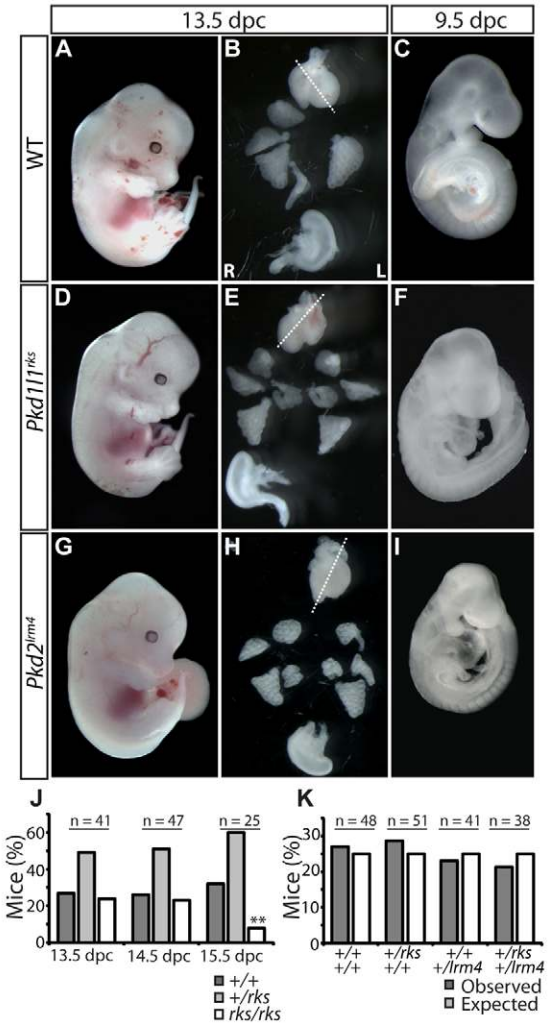

Fig. 2. Gross situs abnormalities in *Pkd1l1*^{rks} and *Pkd2*^{lrm4} embryos. (**A-C**) WT mouse embryo (A) showing left-sided heart apex and stomach and normal lung situs at 13.5 dpc (B), and normal embryonic turning at 9.5 dpc (C). (**D-I**) *Pkd1l1*^{rks} (D-F) and *Pkd2*^{lrm4} (G-I) embryos demonstrate incidences of reversed heart apex and stomach, right pulmonary isomerism and reversed embryonic turning. Dotted lines indicate primary axis of the heart. (**J**) Time-of-death analysis reveals that *Pkd1l1*^{rks} embryos arrest between 14.5 and 15.5 dpc. Two mutant 15.5 dpc embryos were close to death when examined (**). (**K**) *Pkd1l1*^{rks} × *Pkd2*^{lrm4} intercrosses resulted in no departure from Mendelian ratios when genotyped at weaning.

13.5 and 14.5 dpc, normal Mendelian ratios were observed, but by 15.5 dpc a significant drop in the frequency of homozygous embryos was evident (Fig. 2J); only two mutant 15.5 dpc embryos were identified and these were both developmentally delayed and close to death. *Pkd2*^{lrm4} embryos also failed to survive significantly beyond 14.5 dpc, as previously reported (Ermakov et al., 2009) (data not shown).

To determine the precise profile of morphological defects, we analysed genotyped 13.5-14.5 dpc embryos; genetically wild-type (WT) and *Pkd1l1*$^{+/rks}$ embryos proved indistinguishable, exhibiting normal situs and no oedema (Fig. 2A,B). By contrast, all mutant *Pkd1l1*$^{rks/rks}$ embryos analysed (33/33) showed right pulmonary isomerism, with four lung lobes evident on each side (Fig. 2D,E; Table 1); stomach situs and gross cardiac situs, however, showed incidence of both situs solitus and situs inversus (Fig. 2D,E; Table 1). Overt oedema was also present in 25 out of 28 embryos analysed (Table 1). Very similar results were evident for the congenic *Pkd2*$^{lrm4/lrm4}$ mutants (Fig. 2G-I; Table 1): 1 of 38 showed situs solitus lungs, compared with 37 with right isomerism; heart and stomach situs were randomised; 31 of 33 embryos demonstrated obvious oedema (Fig. 2G-I; Table 1). At 9.5 dpc, *Pkd1l1*$^{rks/rks}$ embryos exhibited normal, inverted (Fig. 2F) and indifferent (midline) embryonic turning (Table 1); a mixture of WT and inverted (Fig. 2I) turning was evident in *Pkd2*$^{lrm4/lrm4}$ embryos (Table 1).

Owing to the strong association between defective situs, cardiac defects and oedema (Ramsdell, 2005), we examined cardiac patterning. External patterning of the outflow tract was scored, revealing a significant incidence of apparent double outlet right ventricle (DORV) and transposition of the great arteries (TGA) (Table 2), with ~75% of both *Pkd1l1*$^{rks/rks}$ and *Pkd2*$^{lrm4/lrm4}$ embryos showing overt outflow tract defects. Indeed, the incidence of DORV and of TGA were equivalent in the two mutants. Histological analysis of *Pkd1l1*$^{rks/rks}$ embryos revealed, in addition to evidence of oedema, incidence of ventricular septal defects (VSDs) (see Fig. S2 in the supplementary material), similar to that previously reported for *Pkd2* mutants (Boulter et al., 2001; Ermakov et al., 2009; Pennekamp et al., 2002; Wu et al., 2000). Together, these data demonstrate that the *Pkd1l1*^{rks} and *Pkd2*^{lrm4} phenotypes are highly similar when assessed on an identical genetic background.

Pkd1l1^{rks} embryos do not exhibit defects in kidney development

The established relationship of PKD genes with polycystic kidney disease led us to investigate kidney morphology in *Pkd1l1*^{rks} animals. Mutant *Pkd1l1*$^{rks/rks}$ embryos arrest and die at ~14.5 dpc (Fig. 2J). The kidneys of 14.5 dpc embryos appear normal (data not shown), but it is difficult to analyse cyst formation at this stage; *Pkd1* and *Pkd2* mutant kidney cysts are not readily visualised before 15.5 dpc. However, both *Pkd1*$^{+/-}$ and *Pkd2*$^{+/-}$ adults develop kidney cysts with age (Boulter et al., 2001; Lu et al., 2001; Wu et al., 1998). We therefore investigated the effects of aging *Pkd1l1*$^{+/rks}$ animals, analysing gross pathology, kidney pathology, gross situs and cardiac pathology. We detected no pathology that varied from WT controls in animals aged up to 18 months (see Fig. S3 in the supplementary material; data not shown). Animals doubly heterozygous for *Pkd1* and *Pkd2* show an earlier onset and increased incidence of kidney cysts, reflecting a genetic interaction (Wu et al., 2002). It therefore seemed possible that doubly heterozygous *Pkd1l1*$^{+/rks}$;*Pkd2*$^{+/lrm4}$ animals might show phenotypes affecting L-R patterning. Intercrosses between *Pkd2*$^{+/lrm4}$ and *Pkd1l1*$^{+/rks}$ animals produced progeny at the expected Mendelian frequencies (Fig. 2K); pathological analysis revealed no abnormal kidney, cardiac or situs pathology (data not shown), reflecting no obvious genetic interaction.

Pkd1l1 and *Pkd2* are required to activate asymmetric gene expression

Since morphological L-R asymmetry is prefigured by molecular asymmetries, we next investigated establishment of L-R asymmetric gene expression in the LPM. LPM *Nodal*, expressed between the 3- and 6-somite stages, autoactivates itself and activates its antagonists *Lefty1* and *Lefty2* and the downstream transcription factor *Pitx2* (Shiratori and Hamada, 2006). In WT embryos we detected *Nodal* expression surrounding the node

Table 1. Gross morphological defects in *Pkd1l1*^{rks} and *Pkd2*^{lrm4} embryos

Characteristic	Normal	Inverted	Midline	Right isomerism (oedema)
rks/rks				
Embryonic turning	4/16 (25)	9/16 (56)	3/16 (19)	–
Heart apex	24/32 (75)	7/32 (22)	1/32 (3)	–
Lung situs	0/33 (0)	–	–	33/33 (100)
Stomach situs	6/8 (75)	2/8 (25)	0/8 (0)	–
Oedema	–	–	–	25/28 (89)
lrm4/lrm4				
Embryonic turning	4/11 (36)	7/11 (64)	–	–
Heart apex	15/29 (52)	12/29 (41)	2/29 (7)	–
Lung situs	1/38 (3)	–	–	37/38 (97)
Stomach situs	17/27 (63)	7/27 (26)	3/27 (11)	–
Oedema	–	–	–	31/33 (94)

Embryonic turning scored at 9.5 dpc. Heart apex, lung situs, stomach situs and oedema were scored at 13.5-14.5 dpc. Shown is the number of embryos exhibiting the defect among the total examined, with the percentage in parentheses.

and, from 3-6 somites, in the left, but not right, LPM (Fig. 3A). By contrast, *Pkd1l1*$^{rks/rks}$ embryos showed peri-nodal, but no LPM, expression (Fig. 3B; Table 3). *Lefty2* expression, which normally spatiotemporally echoes that of *Nodal* in the left LPM (Fig. 3D), and *Lefty1* expression in the midline (Fig. 3D), were similarly absent in all mutant embryos analysed (Fig. 3E; Table 3). Asymmetric *Pitx2* expression in the left LPM was detected in WT controls (Fig. 3G) as previously reported (Piedra et al., 1998; Ryan et al., 1998; Yoshioka et al., 1998). However, LPM *Pitx2* expression was absent from 43/44 *Pkd1l1*$^{rks/rks}$ mutants examined (Fig. 3H; Table 3); the remaining embryo demonstrated bilateral LPM expression (Table 3).

The results we describe for *Nodal* and *Lefty2* expression in *Pkd1l1*$^{rks/rks}$ are very similar to data reported for the *Pkd2* null, but there is a significant difference for *Pitx2* as the majority of embryos previously reported showed bilateral *Pitx2* expression (Pennekamp et al., 2002). We therefore analysed expression of situs markers in congenic C3H-*Pkd2*$^{lrm4/lrm4}$ mutant embryos. No expression of *Nodal* or *Lefty2* was detected in the lateral plate (Fig. 3C,F; Table 3), consistent with both the *Pkd1l1*^{rks} data and the previously published *Pkd2* null analysis. However, *Pitx2* expression was also absent from all 17 mutant embryos analysed (Fig. 3I; Table 3), in accordance with data reported here for the *Pkd1l1*^{rks} mutant. Thus, our analysis reveals a failure to activate the Nodal signalling cascade in the LPM of both mutants.

Both their morphology and subsequent normal development over many days, notwithstanding situs-related defects, argue that the LPM, node and midline are structurally normal in *Pkd1l1*^{rks} and *Pkd2*^{lrm4} mutants. We confirmed this by analysing the expression of *Twist* and *Shh*, markers of the LPM and node/notochord, respectively (Echelard et al., 1993; Fuchtbauer, 1995). No difference in expression between WT and mutant embryos was evident (data not shown).

Peri-nodal *Nodal* expression is also asymmetric, with stronger expression on the left than right (Collignon et al., 1996; Lowe et al., 1996); this slightly precedes LPM asymmetry. In WT embryos, we detected asymmetric peri-nodal expression of *Nodal* (Fig. 3A′) beginning at the 2-somite stage (data not shown). By contrast, *Pkd1l1*$^{rks/rks}$ mutant embryos showed no asymmetry of *Nodal* expression at the node (Fig. 3B′). Similarly, *Pkd2*$^{lrm4/lrm4}$ mutant embryos showed no *Nodal* asymmetry (Fig. 3C′). The cerberus-related gene *Cerl2* (also known as *Dand5*) is also asymmetrically expressed at the node, but with higher expression on the right than the left side (Marques et al., 2004; Pearce et al., 1999). In WT embryos, we detected the reported asymmetry of *Cerl2* (Fig. 3J); however, when examining *Pkd1l1*$^{rks/rks}$ (Fig. 3K) and *Pkd2*$^{lrm4/lrm4}$ (Fig. 3L) mutant embryos, we detected no asymmetry in the vast majority of embryos: 18/20 *Pkd1l1*$^{rks/rks}$ and 9/12 *Pkd2*$^{lrm4/lrm4}$ embryos showed L-R symmetrical *Cerl2* expression; 2/20 *Pkd1l1*$^{rks/rks}$ and 2/12 *Pkd2*$^{lrm4/lrm4}$ embryos demonstrated stronger right-sided expression, whereas 1/12 *Pkd2*$^{lrm4/lrm4}$ embryos showed stronger left-sided expression. Together, these data place *Pkd1l1* and *Pkd2* genetically upstream of asymmetric gene expression.

The nodes of *Pkd1l1*^{rks} and *Pkd2*^{lrm4} mutants appear normal

As both gross phenotypic and expression-based data point to a defect originating within the node, we analysed node morphology and function. Three- to four-somite WT and mutant embryos were collected and visualised by scanning electron microscopy. Node size, morphology and cilia length in *Pkd1l1*$^{rks/rks}$ and *Pkd2*$^{lrm4/lrm4}$ mutants were comparable to those of WT embryos (Fig. 4A-G), arguing that the phenotype does not result from abnormal node morphology. Motile cilia at the node generate the nodal flow that establishes embryonic situs (Hirokawa et al., 2006; Shiratori and

Table 2. Heart morphology in *Pkd1l1*^{rks} and *Pkd2*^{lrm4} embryos

Genotype	Wild-type	DORV	TGA	Dextrocardia*
+/+	21/21 (100)	0	0	0
rks/+	39/39 (100)	0	0	0
rks/rks	6/24 (25)	11/24 (46)	7/24 (29)	6/24 (25)
+/+	14/14 (100)	0	0	0
lrm4/+	25/25 (100)	0	0	0
lrm4/lrm4	2/10 (20)	5/10 (50)	3/10 (30)	3/10 (30)

Shown is the number of embryos exhibiting the defect among the total examined, with the percentage in parentheses.
*Embryos showing dextrocardia also exhibited double outlet right ventricle (DORV) and transposition of the great arteries (TGA).

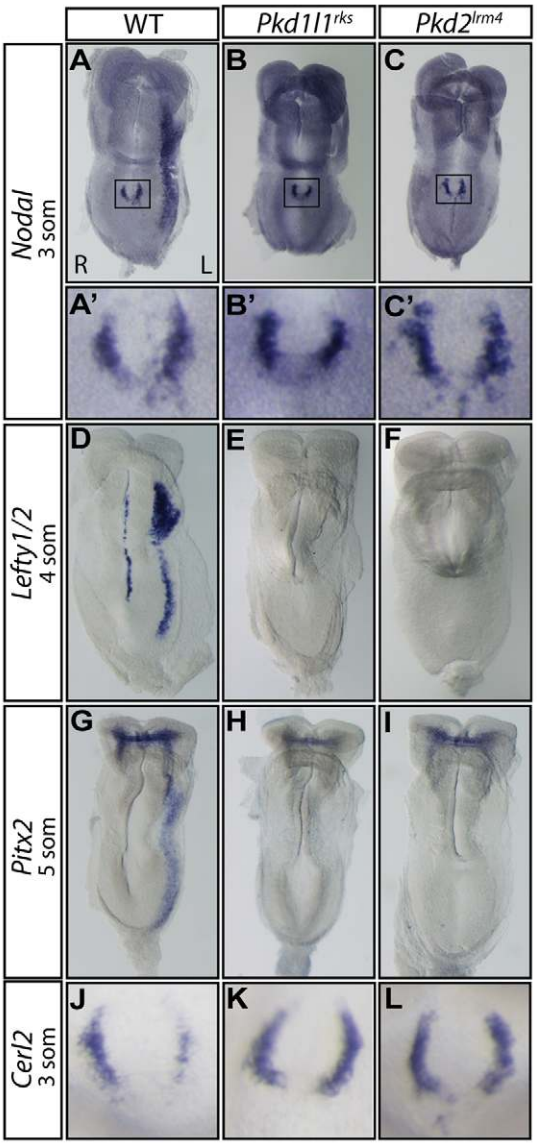

Fig. 3. Failure to activate left-side loci in *Pkd1l1*^{rks} and *Pkd2*^{lrm4} embryos. (**A-C**) *Nodal* mRNA was expressed around the node and in the left lateral plate mesoderm (LPM) in WT mouse embryos, but was absent from the left LPM in *Pkd1l1*^{rks} and *Pkd2*^{lrm4} mutants. Node *Nodal* expression remained symmetrical in mutants (B′,C′) but became more strongly expressed on the left in WT (A′). (**D-I**) *Lefty1/2* (D-F) and *Pitx2* (G-I) expression was absent in both *Pkd1l1*^{rks} and *Pkd2*^{lrm4} mutants. (**J-L**) *Cerl2* mRNA was expressed more strongly on the right side of the node in 3-somite stage WT embryos (J); expression remained symmetrical in mutants (K,L). In all panels, left (L) and right (R) are as indicated in A.

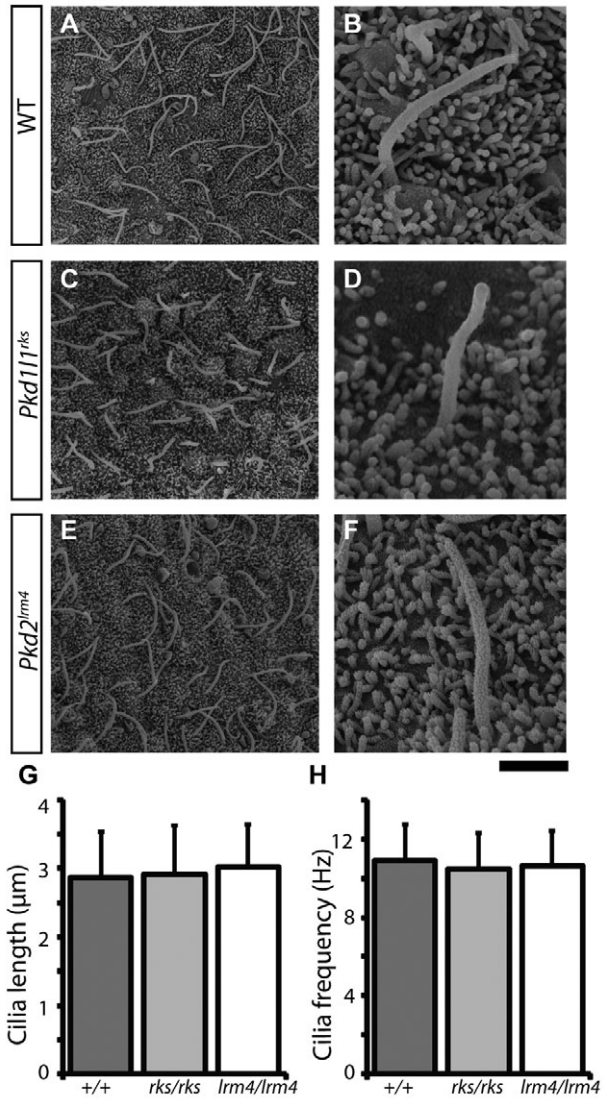

Fig. 4. Node morphology and cilia motility are normal in *Pkd1l1*^{rks} and *Pkd2*^{lrm4} embryos. (**A-F**) Scanning electron micrographs of WT (A,B), *Pkd1l1*$^{rks/rks}$ (C,D) and *Pkd2*$^{lrm4/lrm4}$ (E,F) 8.25 dpc mouse embryos. Scale bar: 5 μm for A,C,E; 1 μm for B,D,F. (**G**) Average cilia length does not vary between WT and mutant embryos. (**H**) Rotational speed of cilia is equivalent in WT and mutant embryos. Error bars indicate s.d.

Hamada, 2006). We therefore visualised cilia motion in WT, *Pkd1l1*$^{rks/rks}$ and *Pkd2*$^{lrm4/lrm4}$ embryos using differential interference contrast microscopy. All embryos analysed showed motile cilia (see Movies 1-3 in the supplementary material). Subsequent frame-by-frame analysis revealed comparable numbers of motile cilia with similar cilial beat frequencies in WT controls, *Pkd1l1*$^{rks/rks}$ and *Pkd2*$^{lrm4/lrm4}$ mutant embryos (Fig. 4H). Our data therefore point to *Pkd1l1* and *Pkd2* acting functionally downstream of cilia motility.

Pkd1l1 is abundantly expressed in the node

If Pkd1l1 and Pkd2 act together in the node to facilitate flow detection in L-R patterning, they must both be expressed in early node-stage embryos (7.75-8.5 dpc). We therefore examined their expression by mRNA whole-mount in situ hybridisation (WISH). Consistent with published data (Pennekamp et al., 2002), we detected broad expression of *Pkd2* throughout the embryo at 7.5-8.5 dpc (data not shown). By contrast, we detected strongly regionalised expression of *Pkd1l1*, with expression in the node, extending into the node crown cells, and in the midline in late streak embryos (Fig. 5A-C), being maintained into early somite stages (Fig. 5D-F). Sectioning of the embryos revealed consistent *Pkd1l1* expression in the outer endodermal layer from 7.5 dpc onwards (Fig. 5C′), with markedly higher expression in the notochordal plate and node (Fig. 5A-C′); this expression was

Table 3. Molecular phenotype of *Pkd1l1*^{rks} and *Pkd2*^{lrm4} embryos

Expression	Normal	Absent	Bilateral
rks/rks			
LPM *Nodal*	0/17	17/17	0/17
LPM/midline *Lefty*	0/9	9/9	0/9
LPM *Pitx2*	0/44	43/44	1/44
lrm4/lrm4			
LPM *Nodal*	0/16	16/16	0/16
LPM/midline *Lefty*	0/19	19/19	0/19
LPM *Pitx2*	0/17	17/17	0/17

Shown is the number of embryos exhibiting the defect among the total examined. LPM, lateral plate mesoderm.

maintained at 8.5 dpc (Fig. 5D-F′). No L-R asymmetry of *Pkd1l1* expression was evident at any stage analysed. No expression was detected with control sense probes (data not shown). *Pkd1l1* and *Pkd2* are therefore co-expressed at the time and place at which it is believed that nodal flow breaks L-R symmetry.

Pkd1l1 and Pkd2 proteins physically interact

As *Pkd1l1* and *Pkd2* are co-expressed in ventral node cells, we hypothesised that their protein products interact to form functional complexes and tested this using immunoprecipitation (IP) assays in human embryonic kidney (HEK) 293T cells. In the absence of functional antibodies against the mouse Pkd1l1 protein, we cloned *Pkd1l1* cDNA and attached a C-terminal GFP tag to create the Pkd1l1-GFP construct (Fig. 6A). This was used in conjunction with the previously published N-terminally tagged Myc-PKD2 (Hanaoka et al., 2000). Lysates from cells transiently transfected with Pkd1l1-GFP and/or Myc-PKD2 were subjected to IP with anti-GFP or anti-Myc antibodies. We detected Myc-PKD2 as either 140 kDa bands (Fig. 6C,D) or as a smear, as found previously (Fig. 6B) (Hanaoka et al., 2000); a specific 140 kDa band was evident at lower exposures (data not shown). Based on the predicted molecular weight of Pkd1l1, we expected to find Pkd1l1-GFP bands at ~315 kDa. However, there were no bands in the 268-460 kDa region on GFP western blots (see Fig. S4A in the supplementary material). Instead, we consistently observed a Pkd1l1-GFP-specific 80 kDa band (see Fig. S4A,B in the supplementary material), which could be enriched by GFP IP. We predicted this to be a Pkd1l1 C-terminal cleavage fragment. Based on the molecular weight as assessed by SDS-PAGE and western blotting, we concluded that the cleavage product is 53 kDa, revealing a cleavage site within the third intracellular loop of the transmembrane region of Pkd1l1 (Fig. 6A, blue arrow). Cleavage at an equivalent position in Pkd1 has recently been described (Woodward et al., 2010), suggesting that this cleavage site is conserved between polycystin-1 family members. During our IP experiments, we found that the Pkd1l1-GFP 80 kDa band, which we named Pkd1l1_53, co-purified with Myc-PKD2 upon GFP or Myc IP (Fig. 6B). In summary, after co-expression of Pkd1l1-GFP and Myc-PKD2, we found that a 53 kDa C-terminal Pkd1l1 cleavage product was able to interact with full-length Myc-PKD2.

PKD1 and PKD2 interact via C-terminal coiled coil (CC) domains (Qian et al., 1997). Pkd1l1 also contains a C-terminal CC domain (see Fig. S1 in the supplementary material), which would still be present in the 53 kDa C-terminal cleavage product; therefore, we examined whether this domain is crucial for the Pkd1l1-PKD2 interaction. To test this, we made a Pkd1l1-GFP construct (Pkd1l1_CC-GFP) consisting of a very short C-terminal Pkd1l1 region containing the final transmembrane domain and the CC domain (Fig. 6A). We co-expressed Pkd1l1_CC-GFP and Myc-PKD2 in HEK 293T cells and performed GFP and Myc IPs on protein extracts. Western blotting revealed a 45 kDa Pkd1l1_CC-GFP band that was successfully enriched by GFP IP (Fig. 6C). IP experiments on doubly transfected samples revealed that Pkd1l1_CC-GFP co-purified with Myc-PKD2 upon GFP or Myc IP, indicative of an interaction. These results suggest that the C-terminal Pkd1l1 CC domain is sufficient for interaction with PKD2. To support this, we mutated a leucine residue within the CC domain to aspartic acid (L2554D), disrupting CC formation (see Fig. S1 in the supplementary material). Under identical IP conditions, the mutant Pkd1l1_CC^{L2554D}-GFP construct did not bind to Myc-PKD2 (Fig. 6D). We also attempted co-IP experiments with Trim71-Flag, a protein that contains a similarly sized CC domain to Pkd1l1 (see Fig. S5A in the supplementary material). We found no evidence of an interaction between Pkd1l1_CC-GFP and Trim71-Flag (see Fig. S5B in the supplementary material), implying that the CC domain of Pkd1l1 shows some specificity for PKD2. Together, these experiments reveal that Pkd1l1 and PKD2 can interact, and that the C-terminal CC domain of Pkd1l1 is sufficient to mediate this interaction.

Pkd1l1 and Pkd2 proteins co-localise to the cilium

As Pkd2 protein is known to localise to nodal cilia (McGrath et al., 2003), we hypothesised that Pkd1l1 would also localise to cilia. To analyse cellular Pkd1l1 localisation, Pkd1l1-GFP and/or Myc-PKD2 were expressed in the ciliated mammalian kidney cell line

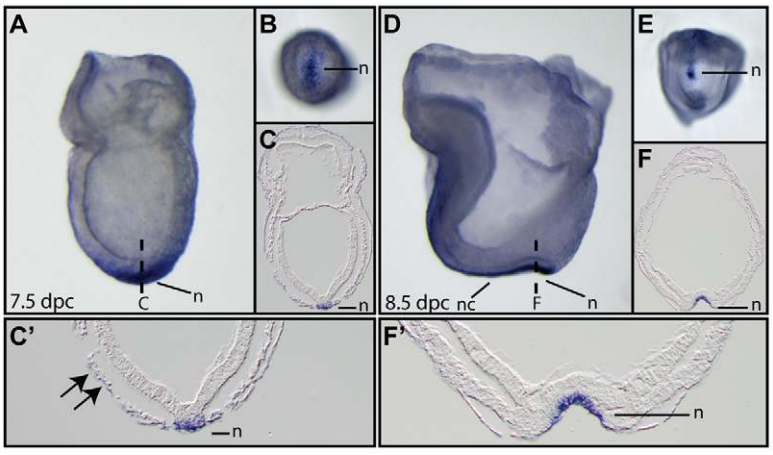

Fig. 5. *Pkd1l1* is strongly enriched in the embryonic node. (**A-F**) *Pkd1l1* mRNA expression visualised by WISH in 7.5 dpc (A-C) and 8.5 dpc (D-F) WT mouse embryos. Highly enriched expression evident in the forming embryonic node (A,B) is clearly localised to the ventral node when viewed in section (C,C′). Higher-magnification views reveal low-level *Pkd1l1* expression in the visceral endoderm (C′, arrows). Enriched *Pkd1l1* expression in the node and midline (D,E) is particularly obvious in sections (F,F′), revealing node expression solely in the ventral layer. n, node; nc, notochord. Planes of section are indicated by dashed lines.

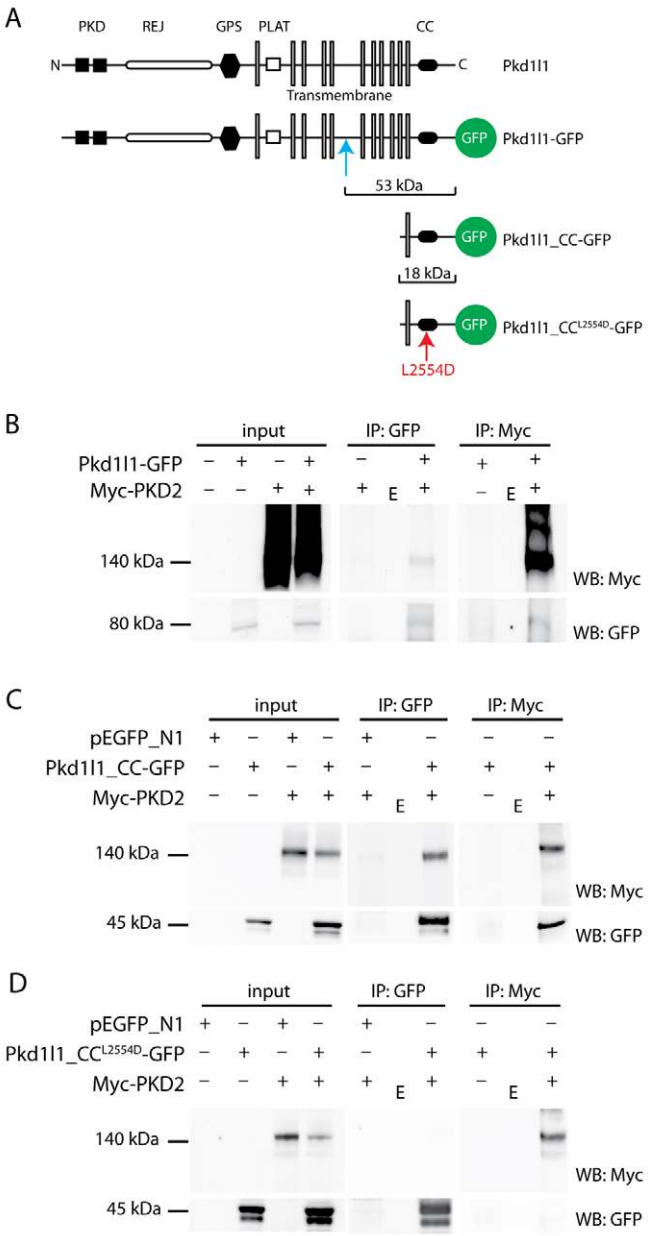

Fig. 6. Pkd1l1 and PKD2 interact via the intracellular coiled coil domain of Pkd1l1. (**A**) Pkd1l1 and the Pkd1l1-GFP, Pkd1l1_CC-GFP and Pkd1l1_CC^{L2554D}-GFP constructs. The cleavage site producing Pkd1l1_53 is indicated (blue arrow). (**B-D**) Immunoprecipitation experiments show that Pkd1l1 and PKD2 interact. (B) A 53 kDa C-terminal Pkd1l1 cleavage product (80 kDa) co-purifies with Myc-PKD2 (140 kDa). (C) The C-terminal coiled coil (CC) domain of Pkd1l1 is sufficient for interaction with PKD2, whereas mutation of the CC prevents the interaction (D). E indicates empty line.

IMCD3. In all experiments, anti-acetylated tubulin staining was used to mark the ciliary axoneme. Mock-transfected control cells revealed a low-level, non-specific, punctate background staining with anti-GFP antibodies and no anti-Myc staining (Fig. 7A). When expressed alone, Pkd1l1-GFP (Fig. 7B) or Myc-PKD2 (Fig. 7C) was localised to the cell body and there was no localisation to the cilia. However, when the two proteins were co-expressed, a reduction in the level of protein detectable in the cell body was accompanied by localisation of the proteins in the cilia (Fig. 7D). When 250 cilia were imaged, four showed Pkd1l1-GFP overlapping the cilial staining of acetylated tubulin in the absence of Myc-PKD2, compared with 163 in the presence of Myc-PKD2 (Fig. 7E). The 35% of cells in which no co-localisation was detected most likely reflects the efficiency of transfection. We further visualised the localisation of both Pkd1l1-GFP and of Pkd1l1_CC-GFP in the presence and absence of Myc-PKD2, visualising only GFP and acetylated tubulin. In the absence of Myc-PKD2, no cilial localisation was evident (data not shown), but in its presence both the full-length Pkd1l1 (Fig. 7F) and the C-terminal Pkd1l1_CC domain (Fig. 7G) were evident in small punctate foci within the cilia. These data support our hypothesis that Pkd1l1-Pkd2 complexes within cilia sense nodal flow and argue that Pkd1l1 requires Pkd2 for cilial localisation.

DISCUSSION

We have identified *rks*, a novel point mutant in *Pkd1l1* that reveals a requirement for this gene in L-R determination. Systematic analysis demonstrates that when variables such as genetic background are removed, *Pkd1l1*^{rks} and *Pkd2*^{lrm4} point mutants show virtually identical morphological and molecular phenotypes. Both lead almost exclusively to right isomerism and failed activation of the left LPM Nodal signalling cascade; asymmetry of gene expression at the node was also affected. However, no defects in node morphology, nodal cilia morphology or function were detected in either mutant, arguing that these genes act between nodal flow and the establishment of asymmetric gene expression. Biochemical analysis shows that the two proteins interact and that the Pkd1l1 C-terminal CC domain alone interacts with Pkd2 protein. Subcellular localisation reveals that both proteins localise to cilia. Together, these data argue that Pkd1l1 is the elusive Pkd2 binding partner in mediating L-R patterning; this disarms a major criticism of the two-cilia hypothesis.

The *Pkd1l1*^{rks} mutation is a single amino acid change at an evolutionarily highly conserved residue lying within the WDFGDGS motif, which was previously identified as the most highly conserved region of PKD domains (Bycroft et al., 1999). The function of the WDFGDGS motif remains unknown; it comprises a linker connecting two β-sheets within a β-sandwich structure. The previous identification of pathological mutations resulting in ADPKD within this motif in PKD domains of human *PKD1* underlines its importance (Rossetti et al., 2007). Intriguingly, atomic force microscopy (AFM) studies have revealed that PKD domains are mechanically very strong and it has been argued that this reflects a role in stress detection (Forman et al., 2005). Subsequent analysis of pathogenic mutations within PKD domains, including mutations within the WDFGDGS motif, showed that these can result in decreased mechanical strength; mutation of the residue neighbouring *rks* results in significant changes in AFM-driven unfolding, consistent with a change in mechanical function (Ma et al., 2009). These findings, along with the molecular modelling that we have performed, suggest that the *rks* mutation destabilises β-sheets within a PKD domain, resulting in reduced mechanical strength. Overall, our observations fit most simply with a model in which the PKD domains of Pkd1l1 are important in sensing or responding to nodal flow.

The question of whether *Pkd1l1*^{rks} is a null mutation is not readily deducible from the domain structure. Recently, however, the characterisation of an engineered *Pkd1l1* null allele has been reported (Vogel et al., 2010); less than one-third of the expected number of homozygotes were identified, implying embryonic

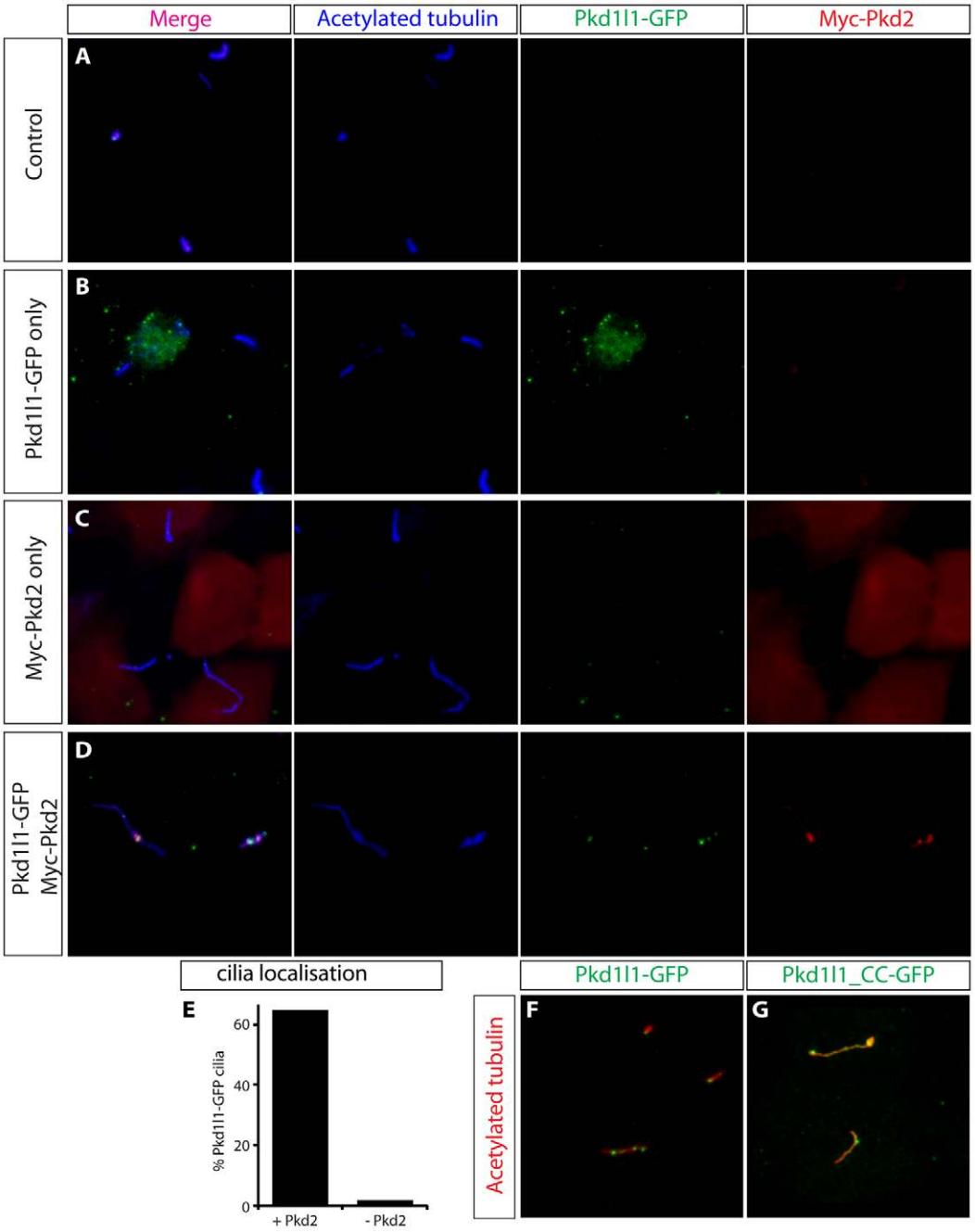

Fig. 7. Pkd1l1 and Pkd2 co-localise to primary cilia. (**A-D**) IMCD3 cells transiently transfected with Pkd1l1-GFP (B), Myc-PKD2 (C), Pkd1l1-GFP and Myc-PKD2 (D), or with no DNA as control (A). Anti-acetylated tubulin staining (blue) marks cilia. Anti-GFP antibody identifies Pkd1l1-GFP (green) and anti-Myc staining marks Myc-PKD2 (red). Merged images (left column) show that, individually, Pkd1l1-GFP and Myc-PKD2 are within the cell body, but localise to the cilia when co-expressed. (**E**) Following transfection of Pkd1l1-GFP, 250 cilia were visualised and the number of cilia showing Pkd1l1 with and without Pkd2 was counted. (**F**,**G**) IMCD3 cells transfected with Pkd1l1-GFP and Myc-PKD2 (F) or Pkd1l1_CC-GFP and Myc-PKD2 (G) and visualised for acetylated tubulin (red) and GFP (green).

lethality. Of those born, one-third demonstrated situs inversus and the remainder situs solitus; no other discernible defects were evident following broad-spectrum phenotyping. Although both mutations clearly affect the establishment of situs, the identification of homozygous viable adults represents a clear phenotypic difference from *Pkd1l1*^{rks}. The two mutations were analysed on different genetic backgrounds (*Pkd1l1*$^{-}$ on a mixed B6;129 and *Pkd1l1*^{rks} on C3H), which we cannot exclude as a source of variation. However, one other interpretation is that *Pkd1l1*^{rks} is a stronger, perhaps dominant-negative, allele. A possible mechanistic explanation of this effect would invoke interaction between Pkd2 and multiple Pkd1 family members. In this scenario, if Pkd1l1 were the major Pkd2 binding partner in the node because of its protein level or binding affinity, then loss of Pkd1l1 protein in the null mutant would allow other family members to partially compensate. The presence of non-functional mutant Pkd1l1^{rks} protein would, by

contrast, maintain the normal interaction with Pkd2, thus preventing other family members from interacting to partially rescue the phenotype. Furthermore, the suggestion that three Pkd2 molecules bind to each Pkd1 molecule (Yu et al., 2009) makes such a model more compelling. Interestingly, Nakaya and colleagues reported Pkd1 protein in mouse nodal cilia (Nakaya et al., 2005), and the physical interaction of Pkd1 and Pkd2 proteins in kidney cilia is well established (Hanaoka et al., 2000; Nauli et al., 2003), showing that such an interaction in the node is possible.

This discussion raises a question about the nature of the *Pkd2*^{lrm4} point mutant that we have analysed. Our data conflict, in part, with the published *Pkd2* null allele (Pennekamp et al., 2002), both in terms of gross morphology and, perhaps most significantly, at the molecular level: *Pitx2* expression was bilateral in two-thirds of the null embryos analysed, and was absent in less than 20%. This might reflect differences in genetic background (*Pkd2*$^{-}$ was analysed on a 129;B6 background, *Pkd2*^{lrm4} on C3H) between the two colonies; indeed, the original *Pkd2*^{lrm4} outbred mice showed a morphological phenotype that more closely resembled that of the null allele (Ermakov et al., 2009). However, we cannot rule out the possibility that multiple Pkd2 family members act at the node, of which Pkd2 is the major player, and that an inactive mutant protein will therefore result in a stronger phenotype than the total loss of that protein. Work to investigate these possibilities is ongoing.

The role of nodal flow in establishing L-R patterning in mammals has become well accepted in the field (for reviews, see Hirokawa et al., 2006; Shiratori and Hamada, 2006), deriving from work on immotile cilia disease (for a review, see Afzelius, 2004) and on mice with ultrastructurally normal, yet immotile, nodal cilia, such as *Dnahc11* and *Dnahc5* mutants (Olbrich et al., 2002; Supp et al., 1997). Similar cilia- and flow-based mechanisms have now been demonstrated in many vertebrate lineages, suggesting that this is a conserved mechanism; only the chicken is reported not to utilise nodal flow (for a review, see Blum et al., 2008). The requirement for *Pkd2* genes in L-R patterning has been demonstrated in both mouse (Pennekamp et al., 2002) and zebrafish (Bisgrove et al., 2005; Schottenfeld et al., 2007), but in both cases the associated interacting partner has remained unidentified. Our work, and that of Kamura and colleagues studying these loci in the medaka fish (Kamura et al., 2011), both point to Pkd1l1 and Pkd2 acting together downstream of nodal flow to mediate L-R patterning, arguing that this is an evolutionarily conserved mechanism.

Multiple models have been proposed to explain the establishment of L-R asymmetry in response to nodal flow. The data we present fit most simply with the two-cilia hypothesis. Within this model, we merely need to invoke co-operation between Pkd1l1 and Pkd2 within sensory cilia at the node, acting to detect flow. Indeed, the identification of human pathogenic ADPKD mutations within WDFGDGS motifs in PKD1 (Rossetti et al., 2007) in combination with the proposed role of PKD domains in force sensation (Forman et al., 2005; Ma et al., 2009; Qian et al., 2005) support this model. By contrast, the morphogen and NVP hypotheses of Hirokawa and colleagues (Nonaka et al., 1998; Okada et al., 2005; Tanaka et al., 2005) do not provide so obvious a niche for Pkd1l1. The presence of a Ca^{2+} signal spreading from the left side of the node in all of these models raises the possibility that Pkd proteins might be involved downstream of flow detection. A third model is proposed by Kamura and colleagues (Kamura et al., 2011). Following extensive analysis, they do not detect immotile cilia in the medaka fish Kupffer's Vesicle (KV; equivalent to the mouse node), and therefore argue that motile KV cilia must act to detect either a morphogen gradient or flow-based stresses. Work from various groups has revealed that motile cilia can and do perform sensory functions, including mechanosensation (for a review, see Bloodgood, 2010). Therefore, it is possible that a modified version of the two-cilia hypothesis exists in medaka fish in which motile cilia are also mechanosensitive; whether motile mouse cilia can be mechanosensitive remains to be determined. We cannot, however, rule out the possibility that a morphogen is involved.

Loss of cilia motility in the node results in randomised situs and stochastic activation of the Nodal signalling cascade in the LPM (Shiratori and Hamada, 2006); left-sided, right-sided, bilateral and failed activation of the cascade are all reported. Modelling has revealed how these results could be produced by stochastic activation of *Nodal* and subsequent reaction-diffusion of Nodal protein and its antagonists Lefty1 and 2 (Nakamura et al., 2006). However, the failed activation of the Nodal cascade in virtually all *Pkd2* and *Pkd1l1* mutant embryos argues that these proteins are required for that stochastic activation. Although the nature of that mechanism is beyond the scope of this study, the restricted expression of *Pkd1l1* argues that this stochastic activation either originates within, or requires signals from, the node. In contrast to the lack of activation of asymmetric lateral plate markers that we report for both *Pkd1l1*^{rks} and *Pkd2*^{lrm4}, zebrafish Pkd2 acts to restrict Nodal (Spaw) to the left lateral plate (Bisgrove et al., 2005; Schottenfeld et al., 2007). Kamura and colleagues demonstrate this difference in function to be more generally maintained in teleosts (Kamura et al., 2011). Whether this difference in action relates to differences in the mechanism by which motility is detected will require further study.

In conclusion, we have identified a Pkd1 family member with a spatiotemporal profile of expression that precisely matches that of a gene predicted to function in the detection of nodal flow. Crucially, its disruption in the *Pkd1l1*^{rks} mutant results in a failure to activate the left-sided Nodal signalling cascade and asymmetric gene expression at the node. No defects were detected in the *Pkd1l1*^{rks} node itself, consistent with Pkd1l1 acting downstream of flow. Moreover, the *Pkd1l1*^{rks} mutant phenocopies defects in *Pkd2*^{lrm4} mutants with respect to situs, the two proteins interact biochemically and they co-localise to the cilium. In light of the known relationship between Pkd1 and Pkd2, our findings argue strongly that Pkd1l1 and Pkd2 jointly comprise a cilia-specific, stress-responsive channel in the node, a conclusion that provides convincing support for the two-cilia hypothesis.

Acknowledgements
We thank Hiroyuki Takeda, Keiichiro Kamura and colleagues for helpful discussion and for sharing their data prior to publication; Jeremy Sanderson (MRC Harwell) for advice and assistance with imaging; Paraskevi Goggolidou (MRC Harwell) for assistance with scanning electron microscopy; Rosario Romero (MRC Harwell) for expert advice; Chris Esapa (MRC Harwell) for reagents and advice; the Histology Department (MRC Harwell) for histology; Colin Davies, Joanne Dorning, Emma Rush and Jackie Harrison (MRC Harwell) for expert husbandry skills; Gregory Germino for providing the Myc-PKD2 construct; Liz Robertson and Martin Blum for providing in situ probes; Colin Johnson for providing IMCD3 cells; and Jenny Murdoch (Royal Holloway) and Victoria Patterson (MRC Harwell) for the Trim71 construct. This work was funded by awards from the MRC to D.P.N. (U142670370 and G0501680) and A.G. (U142684167). Deposited in PMC for release after 6 months.

Competing interests statement
The authors declare no competing financial interests.

Supplementary material
Supplementary material for this article is available at
http://dev.biologists.org/lookup/suppl/doi:10.1242/dev.058149/-/DC1

References

Afzelius, B. A. (2004). Cilia-related diseases. *J. Pathol.* **204**, 470-477.

Bisgrove, B. W., Snarr, B. S., Emrazian, A. and Yost, H. J. (2005). Polaris and Polycystin-2 in dorsal forerunner cells and Kupffer's vesicle are required for specification of the zebrafish left-right axis. *Dev. Biol.* **287**, 274-288.

Bloodgood, R. A. (2010). Sensory reception is an attribute of both primary cilia and motile cilia. *J. Cell Sci.* **123**, 505-509.

Blum, M., Weber, T., Beyer, T. and Vick, P. (2008). Evolution of leftward flow. *Semin. Cell Dev. Biol.* **20**, 464-471.

Bogani, D., Siggers, P., Brixey, R., Warr, N., Beddow, S., Edwards, J., Williams, D., Wilhelm, D., Koopman, P., Flavell, R. A. et al. (2009). Loss of mitogen-activated protein kinase kinase kinase 4 (MAP3K4) reveals a requirement for MAPK signalling in mouse sex determination. *PLoS Biol.* **7**, e1000196.

Boulter, C., Mulroy, S., Webb, S., Fleming, S., Brindle, K. and Sandford, R. (2001). Cardiovascular, skeletal, and renal defects in mice with a targeted disruption of the Pkd1 gene. *Proc. Natl. Acad. Sci. USA* **98**, 12174-12179.

Brennan, J., Norris, D. P. and Robertson, E. J. (2002). Nodal activity in the node governs left-right asymmetry. *Genes Dev.* **16**, 2339-2344.

Bycroft, M., Bateman, A., Clarke, J., Hamill, S. J., Sandford, R., Thomas, R. L. and Chothia, C. (1999). The structure of a PKD domain from polycystin-1: implications for polycystic kidney disease. *EMBO J.* **18**, 297-305.

Collignon, J., Varlet, I. and Robertson, E. J. (1996). Relationship between asymmetric nodal expression and the direction of embryonic turning. *Nature* **381**, 155-158.

Echelard, Y., Epstein, D. J., St-Jacques, B., Shen, L., Mohler, J., McMahon, J. A. and McMahon, A. P. (1993). Sonic hedgehog, a member of a family of putative signaling molecules, is implicated in the regulation of CNS polarity. *Cell* **75**, 1417-1430.

Ermakov, A., Stevens, J. L., Whitehill, E., Robson, J. E., Pieles, G., Brooker, D., Goggolidou, P., Powles-Glover, N., Hacker, T., Young, S. R. et al. (2009). Mouse mutagenesis identifies novel roles for left-right patterning genes in pulmonary, craniofacial, ocular, and limb development. *Dev. Dyn.* **238**, 581-594.

Forman, J. R., Qamar, S., Paci, E., Sandford, R. N. and Clarke, J. (2005). The remarkable mechanical strength of polycystin-1 supports a direct role in mechanotransduction. *J. Mol. Biol.* **349**, 861-871.

Fuchtbauer, E. M. (1995). Expression of M-twist during postimplantation development of the mouse. *Dev. Dyn.* **204**, 316-322.

Gonzalez-Perrett, S., Kim, K., Ibarra, C., Damiano, A. E., Zotta, E., Batelli, M., Harris, P. C., Reisin, I. L., Arnaout, M. A. and Cantiello, H. F. (2001). Polycystin-2, the protein mutated in autosomal dominant polycystic kidney disease (ADPKD), is a Ca2+-permeable nonselective cation channel. *Proc. Natl. Acad. Sci. USA* **98**, 1182-1187.

Hanaoka, K., Qian, F., Boletta, A., Bhunia, A. K., Piontek, K., Tsiokas, L., Sukhatme, V. P., Guggino, W. B. and Germino, G. G. (2000). Co-assembly of polycystin-1 and -2 produces unique cation-permeable currents. *Nature* **408**, 990-994.

Harris, P. C. and Torres, V. E. (2009). Polycystic kidney disease. *Annu. Rev. Med.* **60**, 321-337.

Hirokawa, N., Tanaka, Y., Okada, Y. and Takeda, S. (2006). Nodal flow and the generation of left-right asymmetry. *Cell* **125**, 33-45.

Jing, H., Takagi, J., Liu, J. H., Lindgren, S., Zhang, R. G., Joachimiak, A., Wang, J. H. and Springer, T. A. (2002). Archaeal surface layer proteins contain beta propeller, PKD, and beta helix domains and are related to metazoan cell surface proteins. *Structure* **10**, 1453-1464.

Jones, D. T., Bryson, K., Coleman, A., McGuffin, L. J., Sadowski, M. I., Sodhi, J. S. and Ward, J. J. (2005). Prediction of novel and analogous folds using fragment assembly and fold recognition. *Proteins* **61 Suppl. 7**, 143-151.

Kamura, K., Kobayashi, D., Uehara, Y., Koshida, S., Iijima, N., Kudo, A., Yokoyama, T. and Takeda, H. (2011). Pkd1l1 complexes with Pkd2 on motile cilia and functions to establish the left-right axis. *Development* **138**, 1121-1129.

Karcher, C., Fischer, A., Schweickert, A., Bitzer, E., Horie, S., Witzgall, R. and Blum, M. (2005). Lack of a laterality phenotype in Pkd1 knock-out embryos correlates with absence of polycystin-1 in nodal cilia. *Differentiation* **73**, 425-432.

Koulen, P., Cai, Y., Geng, L., Maeda, Y., Nishimura, S., Witzgall, R., Ehrlich, B. E. and Somlo, S. (2002). Polycystin-2 is an intracellular calcium release channel. *Nat. Cell Biol.* **4**, 191-197.

Logan, M., Pagan-Westphal, S. M., Smith, D. M., Paganessi, L. and Tabin, C. J. (1998). The transcription factor Pitx2 mediates situs-specific morphogenesis in response to left-right asymmetric signals. *Cell* **94**, 307-317.

Lowe, L. A., Supp, D. M., Sampath, K., Yokoyama, T., Wright, C. V., Potter, S. S., Overbeek, P. and Kuehn, M. R. (1996). Conserved left-right asymmetry of nodal expression and alterations in murine situs inversus. *Nature* **381**, 158-161.

Lu, W., Shen, X., Pavlova, A., Lakkis, M., Ward, C. J., Pritchard, L., Harris, P. C., Genest, D. R., Perez-Atayde, A. R. and Zhou, J. (2001). Comparison of Pkd1-targeted mutants reveals that loss of polycystin-1 causes cystogenesis and bone defects. *Hum. Mol. Genet.* **10**, 2385-2396.

Ma, L., Xu, M., Forman, J. R., Clarke, J. and Oberhauser, A. F. (2009). Naturally occurring mutations alter the stability of polycystin-1 polycystic kidney disease (PKD) domains. *J. Biol. Chem.* **284**, 32942-32949.

Marques, S., Borges, A. C., Silva, A. C., Freitas, S., Cordenonsi, M. and Belo, J. A. (2004). The activity of the Nodal antagonist Cerl-2 in the mouse node is required for correct L/R body axis. *Genes Dev.* **18**, 2342-2347.

McGrath, J., Somlo, S., Makova, S., Tian, X. and Brueckner, M. (2003). Two populations of node monocilia initiate left-right asymmetry in the mouse. *Cell* **114**, 61-73.

Meno, C., Ito, Y., Saijoh, Y., Matsuda, Y., Tashiro, K., Kuhara, S. and Hamada, H. (1997). Two closely-related left-right asymmetrically expressed genes, lefty-1 and lefty-2: their distinct expression domains, chromosomal linkage and direct neuralizing activity in Xenopus embryos. *Genes Cells* **2**, 513-524.

Muto, S., Aiba, A., Saito, Y., Nakao, K., Nakamura, K., Tomita, K., Kitamura, T., Kurabayashi, M., Nagai, R., Higashihara, E. et al. (2002). Pioglitazone improves the phenotype and molecular defects of a targeted Pkd1 mutant. *Hum. Mol. Genet.* **11**, 1731-1742.

Nakamura, T., Mine, N., Nakaguchi, E., Mochizuki, A., Yamamoto, M., Yashiro, K., Meno, C. and Hamada, H. (2006). Generation of robust left-right asymmetry in the mouse embryo requires a self-enhancement and lateral-inhibition system. *Dev. Cell* **11**, 495-504.

Nakaya, M. A., Biris, K., Tsukiyama, T., Jaime, S., Rawls, J. A. and Yamaguchi, T. P. (2005). Wnt3a links left-right determination with segmentation and anteroposterior axis elongation. *Development* **132**, 5425-5436.

Nauli, S. M., Alenghat, F. J., Luo, Y., Williams, E., Vassilev, P., Li, X., Elia, A. E., Lu, W., Brown, E. M., Quinn, S. J. et al. (2003). Polycystins 1 and 2 mediate mechanosensation in the primary cilium of kidney cells. *Nat. Genet.* **33**, 129-137.

Nonaka, S., Tanaka, Y., Okada, Y., Takeda, S., Harada, A., Kanai, Y., Kido, M. and Hirokawa, N. (1998). Randomization of left-right asymmetry due to loss of nodal cilia generating leftward flow of extraembryonic fluid in mice lacking KIF3B motor protein. *Cell* **95**, 829-837.

Nonaka, S., Shiratori, H., Saijoh, Y. and Hamada, H. (2002). Determination of left-right patterning of the mouse embryo by artificial nodal flow. *Nature* **418**, 96-99.

Okada, Y., Nonaka, S., Tanaka, Y., Saijoh, Y., Hamada, H. and Hirokawa, N. (1999). Abnormal nodal flow precedes situs inversus in iv and inv mice. *Mol. Cell* **4**, 459-468.

Okada, Y., Takeda, S., Tanaka, Y., Belmonte, J. C. and Hirokawa, N. (2005). Mechanism of nodal flow: a conserved symmetry breaking event in left-right axis determination. *Cell* **121**, 633-644.

Oki, S., Hashimoto, R., Okui, Y., Shen, M. M., Mekada, E., Otani, H., Saijoh, Y. and Hamada, H. (2007). Sulfated glycosaminoglycans are necessary for Nodal signal transmission from the node to the left lateral plate in the mouse embryo. *Development* **134**, 3893-3904.

Olbrich, H., Haffner, K., Kispert, A., Volkel, A., Volz, A., Sasmaz, G., Reinhardt, R., Hennig, S., Lehrach, H., Konietzko, N. et al. (2002). Mutations in DNAH5 cause primary ciliary dyskinesia and randomization of left-right asymmetry. *Nat. Genet.* **30**, 143-144.

Patterson, V. L., Damrau, C., Paudyal, A., Reeve, B., Grimes, D. T., Stewart, M. E., Williams, D. J., Siggers, P., Greenfield, A. and Murdoch, J. N. (2009). Mouse hitchhiker mutants have spina bifida, dorso-ventral patterning defects and polydactyly: identification of Tulp3 as a novel negative regulator of the Sonic hedgehog pathway. *Hum. Mol. Genet.* **18**, 1719-1739.

Pearce, J. J., Penny, G. and Rossant, J. (1999). A mouse cerberus/Dan-related gene family. *Dev. Biol.* **209**, 98-110.

Pennekamp, P., Karcher, C., Fischer, A., Schweickert, A., Skryabin, B., Horst, J., Blum, M. and Dworniczak, B. (2002). The ion channel polycystin-2 is required for left-right axis determination in mice. *Curr. Biol.* **12**, 938-943.

Piedra, M. E., Icardo, J. M., Albajar, M., Rodriguez-Rey, J. C. and Ros, M. A. (1998). Pitx2 participates in the late phase of the pathway controlling left-right asymmetry. *Cell* **94**, 319-324.

Qian, F., Germino, F. J., Cai, Y., Zhang, X., Somlo, S. and Germino, G. G. (1997). PKD1 interacts with PKD2 through a probable coiled-coil domain. *Nat. Genet.* **16**, 179-183.

Qian, F., Wei, W., Germino, G. and Oberhauser, A. (2005). The nanomechanics of polycystin-1 extracellular region. *J. Biol. Chem.* **280**, 40723-40730.

Ramsdell, A. F. (2005). Left-right asymmetry and congenital cardiac defects: getting to the heart of the matter in vertebrate left-right axis determination. *Dev. Biol.* **288**, 1-20.

Rossetti, S., Consugar, M. B., Chapman, A. B., Torres, V. E., Guay-Woodford, L. M., Grantham, J. J., Bennett, W. M., Meyers, C. M., Walker, D. L., Bae, K. et al. (2007). Comprehensive molecular diagnostics in autosomal dominant polycystic kidney disease. *J. Am. Soc. Nephrol.* **18**, 2143-2160.

Ryan, A. K., Blumberg, B., Rodriguez-Esteban, C., Yonei-Tamura, S., Tamura, K., Tsukui, T., de la Pena, J., Sabbagh, W., Greenwald, J., Choe, S. et al.

(1998). Pitx2 determines left-right asymmetry of internal organs in vertebrates. *Nature* **394**, 545-551.
Saijoh, Y., Oki, S., Ohishi, S. and Hamada, H. (2003). Left-right patterning of the mouse lateral plate requires nodal produced in the node. *Dev. Biol.* **256**, 160-172.
Schottenfeld, J., Sullivan-Brown, J. and Burdine, R. D. (2007). Zebrafish curly up encodes a Pkd2 ortholog that restricts left-side-specific expression of southpaw. *Development* **134**, 1605-1615.
Shiratori, H. and Hamada, H. (2006). The left-right axis in the mouse: from origin to morphology. *Development* **133**, 2095-2104.
Supp, D. M., Witte, D. P., Potter, S. S. and Brueckner, M. (1997). Mutation of an axonemal dynein affects left-right asymmetry in inversus viscerum mice. *Nature* **389**, 963-966.
Tabin, C. J. and Vogan, K. J. (2003). A two-cilia model for vertebrate left-right axis specification. *Genes Dev.* **17**, 1-6.
Tanaka, Y., Okada, Y. and Hirokawa, N. (2005). FGF-induced vesicular release of Sonic hedgehog and retinoic acid in leftward nodal flow is critical for left-right determination. *Nature* **435**, 172-177.
Vogel, P., Read, R., Hansen, G. M., Freay, L. C., Zambrowicz, B. P. and Sands, A. T. (2010). Situs inversus in Dpcd/Poll–/–, Nme7–/–, and Pkd1l1–/– mice. *Vet. Pathol.* **47**, 120-131.
Woodward, O. M., Li, Y., Yu, S., Greenwell, P., Wodarczyk, C., Boletta, A., Guggino, W. B. and Qian, F. (2010). Identification of a polycystin-1 cleavage product, P100, that regulates store operated Ca entry through interactions with STIM1. *PLoS ONE* **5**, e12305.
Wu, G., D'Agati, V., Cai, Y., Markowitz, G., Park, J. H., Reynolds, D. M., Maeda, Y., Le, T. C., Hou, H., Jr, Kucherlapati, R. et al. (1998). Somatic inactivation of Pkd2 results in polycystic kidney disease. *Cell* **93**, 177-188.
Wu, G., Markowitz, G. S., Li, L., D'Agati, V. D., Factor, S. M., Geng, L., Tibara, S., Tuchman, J., Cai, Y., Park, J. H. et al. (2000). Cardiac defects and renal failure in mice with targeted mutations in Pkd2. *Nat. Genet.* **24**, 75-78.
Wu, G., Tian, X., Nishimura, S., Markowitz, G. S., D'Agati, V., Park, J. H., Yao, L., Li, L., Geng, L., Zhao, H. et al. (2002). Trans-heterozygous Pkd1 and Pkd2 mutations modify expression of polycystic kidney disease. *Hum. Mol. Genet.* **11**, 1845-1854.
Yates, L., McMurray, F., Zhang, Y., Greenfield, A., Moffatt, M., Cookson, W. and Dean, C. (2009). ENU mutagenesis as a tool for understanding lung development and disease. *Biochem. Soc. Trans.* **37**, 838-842.
Yoshioka, H., Meno, C., Koshiba, K., Sugihara, M., Itoh, H., Ishimaru, Y., Inoue, T., Ohuchi, H., Semina, E. V., Murray, J. C. et al. (1998). Pitx2, a bicoid-type homeobox gene, is involved in a lefty-signaling pathway in determination of left-right asymmetry. *Cell* **94**, 299-305.
Yu, Y., Ulbrich, M. H., Li, M. H., Buraei, Z., Chen, X. Z., Ong, A. C., Tong, L., Isacoff, E. Y. and Yang, J. (2009). Structural and molecular basis of the assembly of the TRPP2/PKD1 complex. *Proc. Natl. Acad. Sci. USA* **106**, 11558-11563.
Yuasa, T., Venugopal, B., Weremowicz, S., Morton, C. C., Guo, L. and Zhou, J. (2002). The sequence, expression, and chromosomal localization of a novel polycystic kidney disease 1-like gene, PKD1L1, in human. *Genomics* **79**, 376-386.